Thermodynamics of freezing in two dimensions: The compressibility of monolayer xenon on graphite

R. Gangwar, N. J. Colella,* and R. M. Suter
Department of Physics, Carnegie-Mellon University, Pittsburgh, Pennsylvania 15213
(Received 15 June 1988; revised manuscript received 16 September 1988)

We give a detailed account of vapor-pressure isotherm measurements of the freezing of monolayer xenon adsorbed on graphite. The carefully equilibrated isotherm data are numerically differentiated to yield the isothermal compressibility. We express the compressibility in terms of the thermodynamic variables of the film: the temperature, T, and the chemical potential, μ. The compressibility anomaly near the freezing transition is found to contain two components: (1) a sharp, $\Delta\mu \sim 2$ K wide peak with a temperature-dependent amplitude which goes to zero near $T = 147$ K and (2) a weak, broad peak with a temperature-independent shape and amplitude. We interpret the sharp peak as indicating a weak first-order transition for $116 < T < 147$ K. In this temperature region, the broad component symmetrically underlies the sharp peak. For $T > 147$ K, where only the broad component persists, the transition appears to be continuous. We compare our results to x-ray scattering and other thermodynamic measurements.

I. INTRODUCTION

The controversy over the nature of melting in two dimensions has lasted seven years now, if one marks the beginning as the publication of model calculations showing that the melting could possibly be a continuous phase transition.[1-3] Common experience would lead one to expect melting transitions to be first order. Landau showed[4] by symmetry arguments that in three dimensions the melting of a crystalline solid into a translationally symmetric fluid must be a first-order transition. All such transitions have been observed to obey this rule. Similar symmetry arguments would apply to two-dimensional crystals.[5] However, crystals with long-range positional order do not exist in two dimensions at finite temperature.[6] Instead, the low-temperature phase of a simple system with short-ranged interactions is expected to have positional correlations which decay algebraically to zero at infinite distance (quasi-long-range order) and long-range bond orientational order.[1-3] The model calculations predict[2,3] that this low-temperature phase can melt into an hexatic phase with short-ranged positional order and quasi-long-range bond orientational order, rather than into a uniform fluid. Since the phases involved in two-dimensional melting differ substantially from the corresponding three-dimensional phases, "common experience" need not apply. Thus, the controversy is not over the *possibility* of continuous melting transitions, but over whether such transitions actually occur in nature.

Rather than give an extensive review of the field, we refer the reader to the recent article by Strandburg[7] which contains a critical review of the field of melting in two dimensions and an extensive set of references. Here, we simply point out that extensive computer simulations[7] as well as numerous experimental techniques[7] have probed the questions as to (i) whether the predicted low-temperature and hexatic phases exist and (ii) whether continuous transitions actually occur. Low-temperature phases with power-law correlations have been verified in several systems,[7-9] and evidence for the existence of hexatic phases appears to be growing.[9,10] Yet the question of the order of the melting transitions remains a point of uncertainty. This question is evidently a subtle one and is the central focus of the present work.

The transition which we have studied is the freezing of monolayer xenon adsorbed on the basal-plane surface of graphite. This is one of the most thoroughly studied examples of a quasi-two-dimensional, continuous symmetry system. The continuous translational symmetry is due to the fact that, at least in the temperature and coverage range of interest here,[11] the xenon periodicity is incommensurate with the graphite substrate periodicity and is only weakly modulated by it.[12] Detailed synchrotron x-ray scattering measurements of the freezing transition have shown that near the phase boundary, the positional correlation length continuously evolves to values as large as 2000 Å,[13] indicating that the freezing transition is at most weakly first order over a substantial temperature range. Experiments on exfoliated graphite,[12,14] at temperatures below 120 K, have resolved composite line shapes in a narrow coverage interval, indicating coexistence of liquid and solid phases and, thus, a first-order transition. Such coexistence is not observed above 120 K, leading to the conclusion that the transition is continuous at higher temperatures.

In addition to the scattering measurements, detailed thermodynamic data have been collected on the xenon on the graphite melting transition. A previous vapor-pressure isotherm experiment,[15] covering essentially the same temperature range as the present work, concludes that the transition remains first order up to 155 K. This conclusion is based on an estimate of the width in chemical potential of the steep region of the isotherms. Our data are quite similar to Tessier's,[15] but the low noise level of our data allows us to carry out a more sensitive analysis of the transition signature and we conclude that the transition becomes continuous at about 147 K. Heat-capacity data have recently been collected on a high-quality exfoliated substrate.[16] However, these measurements probe a higher coverage region of the phase diagram than that discussed here. Previous heat-capacity measurements were restricted largely to the submonolayer region.[17]

The central conclusion of our work is that the xenon freezing transition is weakly first order for $115 \le T \le 147$ K and is continuous for $147 \le T \le 155$ K. This conclusion is based on a clear observation of a first-order transition signal which we are able to follow as the transition weakens. In particular, our data yield quantitative values for the two-dimensional isothermal compressibility in the region of the freezing transition (our data are taken along isothermal paths, starting in the disordered phase and, with increasing density, move into the ordered phase; hence, we refer to freezing rather than melting). Above $T = 155$ K, the formation of a second layer gas begins to interfere with the freezing transition signal, and it is difficult for us to extend our analysis; the transition may remain continuous at higher temperatures. An account of our earlier data has been given;[18] conclusions reached there are consistent with those presented here. In this paper, we include (i) new data taken with an improved apparatus, (ii) a more detailed description of the data, and (iii) additional evidence supporting our conclusions.

II. EXPERIMENTAL CONSIDERATIONS

A. Apparatus

The data presented below were collected using a volumetric vapor-pressure isotherm technique.[19] Data using two different gas-handling systems are included. The systems are operationally similar; details[20] are presented in Ref. 19. The earlier system[18] is constructed of $\frac{1}{4}$-in. stainless-steel plumbing and has a vapor volume (excluding the sample cell) of 55 cm^3. To obtain greater precision along the high-temperature part of the melting line, we constructed a mini-gas-handling system (mini-gh) using $\frac{1}{8}$-in. stainless steel plumbing; the volume of this system is 10.5 cm^3. The mini-gh has separate temperature regulation of the gas-handling box and of the MKS Baratron pressure gauges. Each system was connected to the same sample cell (with volume 2.9 cm^3), housed in a Displex cryostat. Using the algorithm detailed in Ref. 19, each isotherm cycle requires about 40 min to complete; the typical equilibration time after letting a dose of gas into the sample cell is 30 min. In the next section, we present evidence that our procedure does indeed measure the equilibrium state of the adsorbed film.

B. Sample

Our sample is a 1-g piece of Union Carbide's ZYX exfoliated graphite with a surface area, computed from the coverage at one commensurate monolayer of Kr, of 1.62 m^2. ZYX has the largest surface coherence length of commercially available exfoliates ($\sim$2000 Å),[21] and is the substrate on which the bulk of the x-ray scattering measurements of Xe on graphite have been made. Recent scattering work has made use of even higher-quality single-crystal substrates.[13] Our sample, originally 2.5 cm $\times$ 2.5 cm $\times$ 0.3 cm, was cut into two equal rectangular pieces with the aim of improving equilibration times. The sample was baked in a quartz tube at 850 °C for several hours, after which the pressure was $\sim 10^{-6}$ Torr. Several bake outs were performed over the course of data taking with no observable change in isotherm shapes.

C. Precision

The expected relative precision (i.e., statistical noise level) of coverage measurements can be estimated as follows. Usually, the primary source of noise is in the pressure measurement; pressure noise of magnitude δP leads to noise in the coverage

$$\delta P/P = \delta N_v/N_v = \delta N_a/N_v = \delta\Theta/(N_v/N_{\mathrm{ML}}) , \qquad (1)$$

where N_v is the number of atoms in the vapor phase, N_a is the number of atoms adsorbed, Θ is the coverage in monolayer units, and N_{ML} is the number of atoms in one monolayer. Now,

$$N_v/N_{\mathrm{ML}} = (P/N_{\mathrm{ML}}k_B)\sum_i (V_i/T_i) , \qquad (2)$$

where V_i and T_i are volumes and temperatures associated with different sections of the apparatus, k_B is Boltzmann's constant (we neglect thermal transpiration corrections for the moment). Taking the sample cell temperature, T_{sc}, to be 125 K and other temperatures to be 300 K and using $N_{\mathrm{ML}} = 9\times 10^{18}$ as is appropriate for our sample, we obtain

$$\delta\Theta = 0.28\delta P$$

for the large gas-handling system, and

$$\delta\Theta = 0.049\delta P$$

for the min-gh system; pressures are expressed in Torr. The Baratron gauges are stable to better than 10^{-4} of the full-scale reading, P_{FS}; we use gauges with P_{FS} of 1, 10, 100, and 1000 Torr. Thus, our coverage noise ranges, in the mini-gh system, from 5×10^{-6} to 5×10^{-3} ML. Note that these are not absolute accuracies but only estimates of the smallest resolvable features. Note also that at high temperatures and coverages, desorption due to small fluctuations in the sample cell temperature can generate pressure noise which is large compared to the above figures (see the Appendix).

D. Data analysis

The pressure in the sample cell is obtained by multiplying raw pressure measurements in the room-temperature gas-handling system by a thermal transpiration correction factor. We use the commonly accepted Takaishi and Sensui[22] formula and their coefficients for Xe. As we move along the Xe melting line, the magnitude of the transpiration correction at the transition varies from 16% at $T=115$ K to 2.5×10^{-5}% at $T=160$ K. The correction at the transition is less than 1% at and above $T=130$ K. Since we observe an anomaly in the melting signature which is temperature independent over this entire range, the correction factor can be assumed to be adequate.

Inevitably, there is a slow pressure drift in our gas-handling system due presumably to residual outgassing. In both gas-handling systems, this drift is in the range of $10^{-7}-10^{-8}$ Torr/sec or less (note that the same pressure drift in the mini-gh system implies a considerably lower contamination rate). We have measured the sample temperature dependence of the pressure drift and found it to be independent of temperature down to $T\sim50$ K, where the rate drops quickly.[18(b)] We conclude that the molecular species responsible for the drift do not appreciably adsorb on the sample at the temperatures involved in the present work ($T>100$ K). We therefore simply subtract from our pressure measurements a contribution proportional to the time, since the system was last evacuated to low pressure ($\leq10^{-7}$ Torr). The proportionality is determined by measuring the system pressure over a long period during which no gas is admitted. The drift correction is negligible near the freezing transition for temperatures above 130 K.

For much of the analysis appearing below, we present our data in the form of the two-dimensional isothermal compressibility, K_T:

$$K_T=\Theta^{-2}\partial\Theta/\partial\mu \ , \tag{3}$$

with μ being the chemical potential of the coexisting vapor and adsorbed Xe:

$$\mu(T,P)=k_B T\ln[P/P_0(T)] \ , \tag{4}$$

where $P_0(T)$ is the quantum pressure. As discussed in Ref. 19, we obtain a finite difference approximation to the derivative in (3) by taking differences between neighboring isotherm data points. Due to the low noise in the coverage measurements and the small steps taken in P, we obtain accurate values for K_T.

Two limitations will be seen in the data: (i) at high pressures (which are encountered at high temperatures), the precision in measuring Θ is degraded, quickly increasing the noise in K_T, and (ii) at first-order transitions, K_T becomes large and, using our algorithm which lets in a constant number of xenon atoms per isotherm cycle, the change in chemical potential between successive data points, $\Delta\mu$, becomes small since there is only a small change in vapor pressure; the noise in this difference between two large numbers becomes significant, leading to large uncertainties in K_T. Due to (i), our ability to quantify the melting anomaly at high temperatures is limited. Due to (ii), we measure the width of the first-order coexistence region directly from the coverage data rather than by measuring the height of the peak in K_T; on the other hand, we use K_T to deduce the presence of a first-order region and to measure the extent of heterogeneous smearing of the first-order transition.

What phase transition signals can we expect to observe in our isothermal scans? In crossing a first-order coexistence region, we expect the coverage to increase at a fixed value of the chemical potential. Thus, ideally, K_T should exhibit a delta-function peak whose strength is proportional to the density difference between the coexisting phases. On real substrates, some heterogeneous and finite-size smearing can be expected; on high-quality exfoliated graphites, the smearing is typically a few kelvin in chemical potential.[23–26] An important point to note is that, at least if heterogeneity is the dominant source of smearing, the shape and width of the first-order transition signal should be fixed when isothermal data are plotted against chemical potential.[23,26] Only the peak height varies with the density difference between coexisting phases.

At higher-order transitions, a weaker anomaly in K_T is expected. For second-order transitions, either a power-law divergence or cusp can be expected depending on the type of transition and the values of critical exponents. In the two-dimensional melting problem, the continuous melting theory of Kosterlitz, Thouless, Halperin, Nelson, and Young[1–3] (KTHNY) describes a transition of infinite order. In this case, no singularity is expected in finite-order derivatives of the free energy and, hence, in K_T. However, the heat capacity is expected to show a nonsingular bump *near* the transition, predominantly in the melted phase.[2,3] This bump is a Schottky-type anomaly associated with the unbinding of dislocation pairs. Since K_T and the heat capacity are both second derivatives, one might naively guess that K_T would show a similar anomaly associted with the same phenomenon.[27] Regardless of the details, one expects to see at most a nonsingular signature of the transition. Finally, if, as we believe, there is a multicritical point in the phase diagram which separates first-order and continuous transition regions, a behavior characteristic of this point, possibly quite distinct from KTHNY theory, can be expected. Unfortunately, there has been little theoretical progress in understanding the behavior near such a multicritical point; we do not know whether to expect a singular or nonsingular thermodynamic response.

III. RESULTS

In Fig. 1(a), we show a broad scale vapor-pressure isotherm of xenon on ZYX graphite taken at $T\sim105.5$ K. The chemical potential is computed from the vapor pressure, according to Eq. (4). The data span the coverage range from zero to the onset of the second monolayer; the vapor pressure varies by more than three decades. The coverage is essentially in units of the standard "B_1" point monolayer definition,[28] although we have determined this number in a somewhat different way (see below). In Fig. 1(b), we display the isothermal compressibility computed according to Eq. (3). Note that K_T also spans more than three decades and displays clear signatures of phase transitions. As we move in the direction of increasing chemical potential, the isotherm first displays a large, nearly vertical rise in coverage corresponding to the $2D$ gas-liquid transition.[28] Next, near $\mu=-2950$ K, the isotherm displays the freezing (liquid-solid) transition[15,28] whose entire density anomaly is only $\sim5\%$ of one mono-

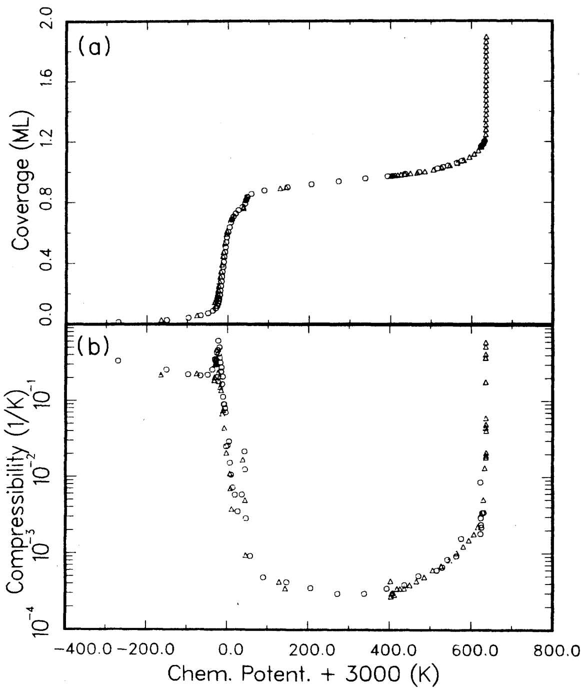

FIG. 1. Vapor-pressure isotherm for xenon on ZYX graphite at 105.4 K. The data are combined from two separate runs; circles represent the data at 105.456(1) K and triangles at 105.435(1) K. Quoted temperature errors are the standard deviations of measurements taken after each isotherm data point and thus represent a measure of temperature stability; absolute temperatures should be accurate to better than 0.1 K. (a) The coverage in monolayer units and (b) the compressibility in inverse kelvin. The horizontal scale is the chemical potential deduced from the ideal gas formula.

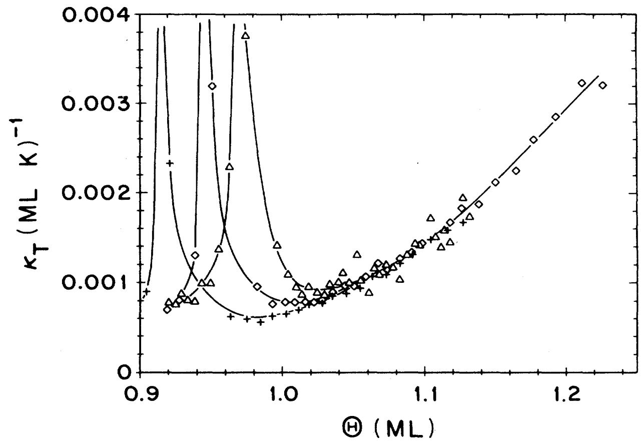

FIG. 2. The compressibility vs coverage in the region near freezing and into the beginning of second layer formation. Symbols are as follows: pluses for $T=105.5$ K, diamonds for $T=150.0$ K, and triangles for $T=152.1$ K. Lines are guides to the eye. Liquid-solid transition peaks in K_T are truncated.

layer. Above the freezing transition, the coverage remains almost constant, growing with a weak linear dependence on chemical potential. At corresponding values of μ in Fig. 1(b), we see that the compressibility falls precipitously after the freezing transition and remains low over a large interval of chemical potential. At the highest values of chemical potential in the figure, there is a first-order condensation transition in the second monolayer, as evidenced by the vertical rise in the coverage and the large peak in K_T. The liquid-solid transition occurs at 0.0022 Torr and the second-layer transition at 0.1 Torr.

In Fig. 2, we display the compressibility plotted against coverage for three isotherms which reach the beginning of second-layer formation. The compressibility scale is highly expanded to show the details of the initial increase associated with the formation of a second layer gas. In the region $0.9<\Theta<1$, the monolayer freezing transition takes place; only the tail of the freezing peak in K_T is observed in this figure (see Fig. 1 and the discussion below). At higher coverage, one sees the compressibility increase as an equilibrium second-layer gas forms; this takeoff eventually "shorts out" the signal from the first monolayer. At the highest temperature shown, the monolayer freezing transition takes place quite close to the beginning of second-layer formation; at even higher temperatures, we are not able to cleanly separate the two signals. In the lowest-temperature data, at $T=105$ K, the compressibility begins to increase essentially at $\Theta=1$ ML, as one would like for a conceptually correct definition of a monolayer.[29] At higher temperatures, the takeoff begins at somewhat higher coverages, between 1.02 and 1.04 ML. Interestingly, K_T, at constant coverage, is independent of temperature in the second-layer gas region; evidently, the second-layer gas is far from being ideal, since in that case one would expect $K_T \sim T^{-1}$ at constant coverage.

A. Behavior near the melting transitions

We have studied the freezing transition with isotherms that scan a relatively narrow range in chemical potential with high resolution. For example, in Fig. 3, we display the coverage, Θ, and compressibility, K_T, in a broad region around the freezing transition plotted against the chemical potential deviation from the position of the peak in K_T. The transition anomaly has an approximately symmetrical shape.[15] In Fig. 3(b), we see that the compressibility is large in a narrow range of chemical potential, $|\Delta\mu|\leq 2$ K, and shows the behavior of the uniform liquid ($\Delta\mu\leq -40$ K) or solid ($\Delta\mu\geq 25$ K) phases well outside this region. Below, we analyze the transition by examining the region $\Delta\mu=\pm 50$ K.

It is somewhat surprising that, as the temperature is raised (and, correspondingly, the coverage at which freezing takes place rises), the compressibilities of the liquid and solid phases, extrapolated to the transition, become essentially equal. In Fig. 4 we show estimated pure phase compressibilities at the transition, obtained from a linear extrapolation of data within $\Delta\mu=\pm 40$ K of the transition to the chemical potential at which the peak compressibil-

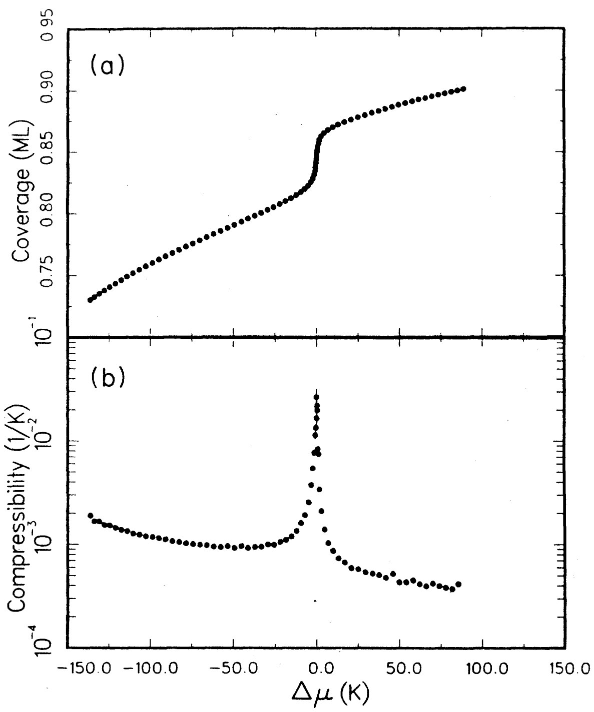

FIG. 3. The melting transition at 122.499(3) K plotted against the chemical potential. (a) displays the coverage and (b) the compressibility. The chemical potential corresponding to the peak compressibility has been subtracted.

ity is observed (see Fig. 8 below). In the vicinity of $T = 147$ K, the compressibilities become essentially equal, although the noise on this highly expanded scale becomes quite large. $T = 147$ K is also the temperature where we estimate, based on considerations described below, that the melting transition becomes continuous.

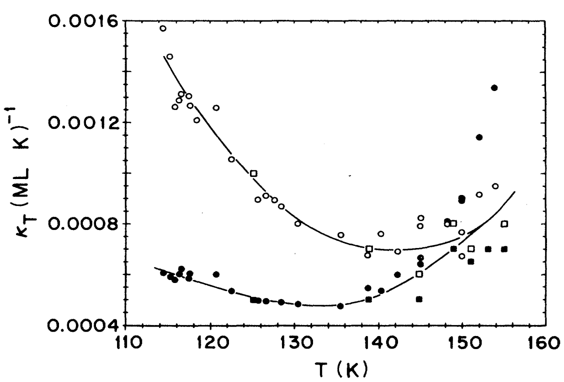

FIG. 4. Pure phase compressibilities extrapolated to the freezing transition at different temperatures. Circles are data from the large gas-handling system; squares are data from the mini-gas-handling system. Open symbols are the liquid phase, solid symbols are from the solid phase. The solid lines are guides to the eye. The scatter in the data at low temperatures is largely due to extrapolation uncertainties (see text), whereas at high temperatures the data become noisy because of the large vapor pressures.

B. Phase diagrams

In Fig. 5(a), we display the chemical potential-temperature phase diagram. We include the data of Tessier[15] and of Thomy and Duval.[28] Clearly, above 120 K, our data and those of Tessier agree within measurement precision. Below 120 K, the transition vapor pressure is below 0.01 Torr, and thermal transpiration corrections and pressure drifts become important. Our absolute pressure measurement is degraded here; we see no reason to expect the phase boundary to deviate from the linear behavior seen at higher temperatures. Also shown in Fig. 5(a) is the chemical potential at which we see the compressibility start to increase, indicating the beginning of second layer formation, as is also seen in Fig. 2. Note that *this line is not a line of phase transitions,* but rather only the onset of a visible second-layer effect. Over most

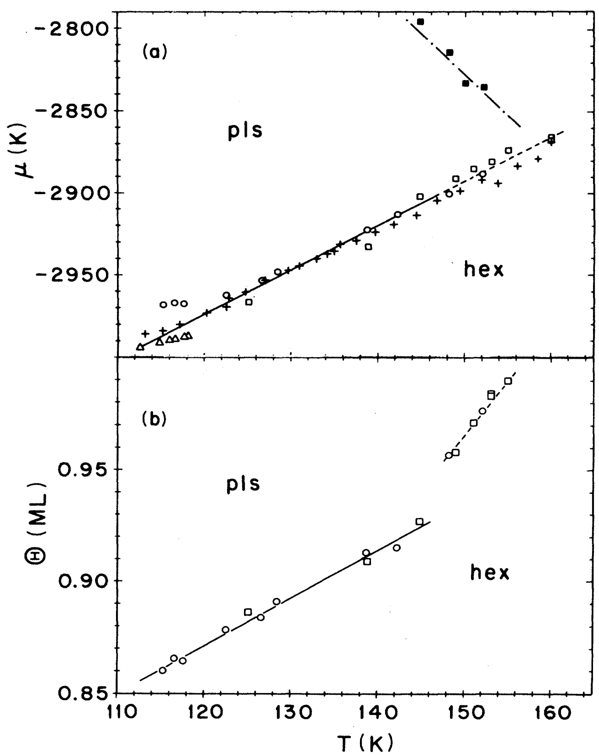

FIG. 5. Phase diagrams near the monolayer freezing transition. (a) shows the chemical potential-temperature diagram and (b) the coverage-temperature diagram. pls stands for the power-law solid phase, hex for the hexatic phase. Circles are from the large gas-handling (gh) system, squares are from the mini-gh system; in addition, the crosses in (a) are from Tessier (Ref. 15) and the triangles are from Thomy and Duval (Ref. 28). Lines are guides to the eye, with solid lines representing first-order and dashed lines continuous transitions. In (a), the solid squares and the dot-dashed line represent the *onset* of second-layer formation as deduced from plots of the type shown in Fig. 2. In (b), the coverage is plotted on an expanded scale. The points are the coverages at which the isotherms achieve their maximum slope and thus represent the approximate middle of the coexistence region for $T < 147$ K and the center of the weak anomaly for $T > 147$ K.

of the temperature range of the experiment, the first-layer melting anomaly is unaffected by a second-layer population since the anomaly is less than 40 K wide in chemical potential.

Figure 5(b) shows the coverage-temperature phase diagram. In the first-order region (solid line) the points represent the estimated midpoint of the coexistence region. Our data are completely consistent with those of Tessier[15] when we scale her coverage measurements to our monolayer units.[18(b)] The coverage rises slowly and essentially linearly with temperature up to at least $T=143$ K. Above $T=148$ K, the boundary rises more rapidly and appears to be offset from the lower-temperature line. The evidence for an anomally in the phase boundary is quite strong. On the other hand, the data are not sufficient to determine the shape of the intersection region near $T=147$ K. It is important to note that some form of anomaly in the phase boundary is consistent with, and suggestive of, the existence of a multicritical point, since scaling theory predicts that a line of continuous transitions should intersect a first-order coexistence region, generally at some nonzero angle.[30] Further evidence for the existence of a multicritical point is presented below.

C. The melting transition

We show in Fig. 6 the melting transition region of the set of isotherms collected using the mini-gh system. The transition chemical potential has been subtracted in order to align the data. The increase in the transition coverage can be seen clearly, as can the fact that the density difference between liquid and solid phases decreases with increasing temperature. The identical trends are seen in Ref. 15. At $T=125.1$ K, we have tested the reversibility of our isotherm procedure. The +'s represent a "desorption" isotherm in which we start at a coverage above the freezing transition and pump gas out of the system in a stepwise procedure. After 33 desorption steps, the reverse run agrees with the forward run to within 0.1% of a monolayer. We conclude that our equilibration procedure does indeed yield information about the equilibrium state of adsorption at each vapor pressure. Also, we show two isotherms at $T=153$ K in order to demonstrate the repeatability of our procedure; these two data sets overlay to better than 0.1% of a monolayer in spite of the long time between measurements. Below, we analyze the isothermal compressibility derived from the data in Fig. 6 and from the original data of Ref. 18.

Figure 7 shows the compressibility anomalies near the monolayer melting transition for eight different isotherms. Since the transition chemical potential increases monotonically with temperature, the data on the extreme left are the lowest in temperature and the data on the extreme right are the highest in temperature. Obviously, the dominant trend is the decrease in the peak height with increasing temperature. It can also be noted that the shape of the tail of the anomaly is essentially independent of temperature throughout the entire region of our study and, at high temperatures, the "tail" constitutes the whole anomaly. The decrease in area under the anomaly corresponds to the decrease in density difference between the liquid and solid phases seen in Fig. 6. In the following, we attempt to quantify these observations.

In Fig. 8(a) we show an overlay of the tails of the compressibility anomaly at low temperatures. The verti-

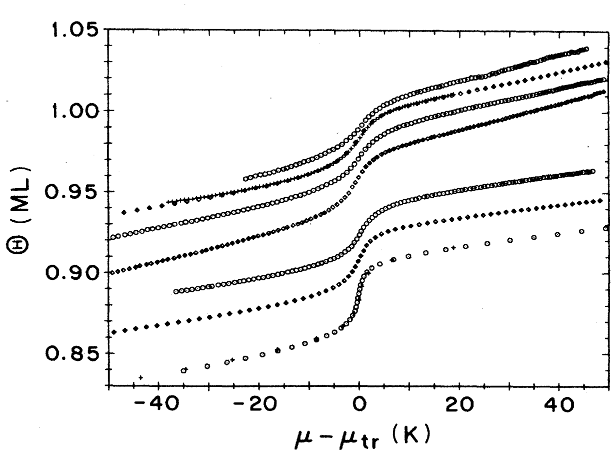

FIG. 6. Isotherms in the region near the freezing transition, collected with the mini-gh system. Starting from the bottom, temperatures are 125.1 (+'s represent desorption data; see text), 138.8, 144.8, 148.9, 151.0, 153.0 (two data sets collected more than a month apart), and 154.9 K. The data have been aligned in chemical potential by subtracting the value at the point of maximum slope.

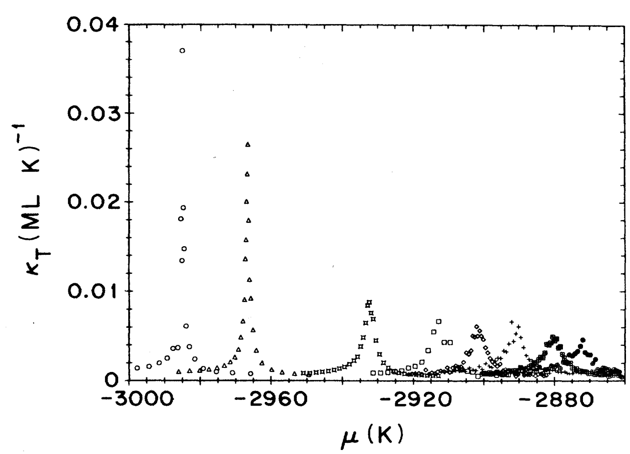

FIG. 7. The melting transition compressibility anomalies from representative data sets spanning the temperature range of our study: From left to right, the temperatures are 116.5, 125.1, 138.8, 142.2, 144.8, 148.9, 151.0, and 154.9 K. The 116.5- and 142.2-K data were collected with the large volume gas-handling system; others used the mini-gh system. Only data from a roughly $\Delta\mu=20$ K region around the peak are included. The lowest-temperature peak is larger than shown, having been truncated so that the higher-temperature peaks can be seen clearly. In fact, we do not quantitatively resolve the peak heights below about 125 K. Nevertheless, one can see the dramatic decrease in peak height as the temperature increases and the roughly temperature-independent behavior at high temperature.

cal scale is chosen so that only the tail region appears—data points in the center of the peak have been truncated. On the liquid side ($\Delta\mu<0$), one can see the slow evolution of the uniform phase compressibility, while on the solid side ($\Delta\mu>0$), the compressibility is essentially independent of temperature (see Fig. 4). The surprising feature is that, after accounting for the liquid phase temperature dependence, the tails of the peaks overlap to within the statistics of the data. Thus, in contrast to the dramatic decrease of peak height seen in Fig. 7, the tail shape is temperature independent. Figure 8(b) shows the corresponding overlay for high-temperature data. Here, the entire anomaly is shown with no data truncated in the center. Within statistics, the data overlap completely. In fact, the data of Figs. 8(a) and 8(b) also overlay in the same manner.

We deduce from Figs. 7 and 8 that the compressibility anomalies at low temperatures contain two separable components: (i) A sharp, $\Delta\mu\sim 2$ K wide peak which decreases in strength with increasing temperature. We attribute the sharp peak in K_T to a heterogeneity broadened first-order phase transition. The width of this peak is similar to the observed adsorption potential heterogeneity on several exfoliated graphites.[23–26,31] In particular, this value corresponds closely to the value we have seen in previous work with Kr on our sample of ZYX.[26] (ii) An apparently nonsingular, broad anomaly which underlies the first-order peak and which has a shape and an amplitude which are independent of temperature. This contribution remains as the sole contributor above $T\sim 147$ K.

Next, we estimate the width, $\Delta\Theta_1$, of the first-order coexistence region as a function of temperature. Given the observed composite compressibility peak shape, obtaining this estimate is analogous to extracting the integrated intensity of a resolution limited Bragg scattering peak in the presence of a diffuse background. Here, our "Bragg peak" is the first-order delta-function in K_T, our resolution is the heterogeneity width, and the diffuse background is the weak anomaly in addition to the pure phase compressibility. In contrast to the scattering problem, our data in a large compressibility peak are less accurate than in the background region[19] so we choose not to do a fit to the first-order peak. Instead, to extract $\Delta\Theta_1$ we utilize the fact that our direct measurement gives the coverage and we do the following: First, as shown in Fig. 9, we interpolate from the isotherm the total coverage difference, $\Delta\Theta$, at $\Delta\mu=\pm 1$ K from the point of maximum compressibility. Then we subtract $\Delta\Theta_{\text{pure}}$, the contribution due to the uniform phase backgrounds. This is ob-

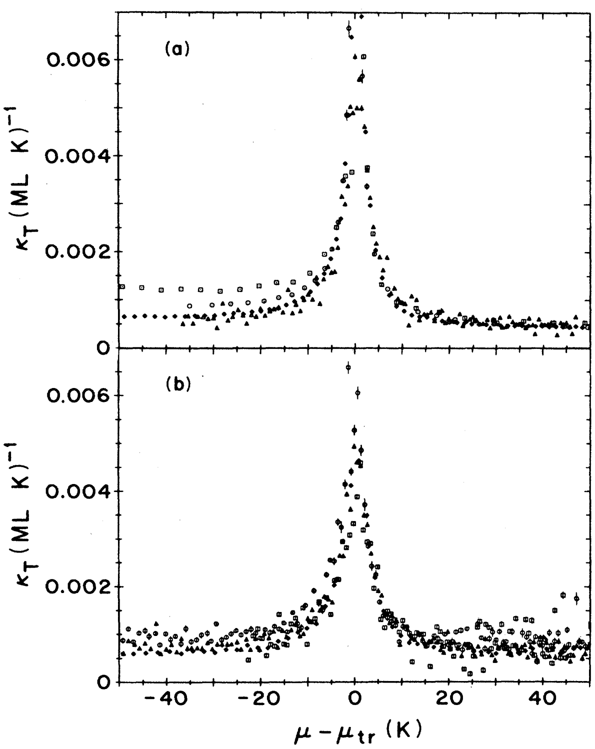

FIG. 8. Overlays of the compressibility anomalies showing only the lower region of the ordinant used in Fig. 7. (a) shows low-temperature data in the region $115<T<145$ K and (b) shows data in the region $147<T<155$ K. Symbols are as follows: In (a), squares are 115.8, circles are 125.1, diamonds are 138.8, and triangles are 144.8 K and in (b), circles are 148.8, triangles are 151.0, diamonds are 153.0, and squares are 154.9 K. As seen from Fig. 7, each of the data sets in (a) have been truncated in the center of the anomaly, whereas the data sets in (b) show the entire peak structure. Overlaying (a) and (b) demonstrates that the tail structure is independent of temperature over the entire region studied. In (a), the evolution of the liquid-phase compressibility is seen on the left side of the anomaly. Note also that the slight increase in K_T seen in the solid phase (at the right) for the data at $T=154.9$ K represents the beginning of second-layer formation.

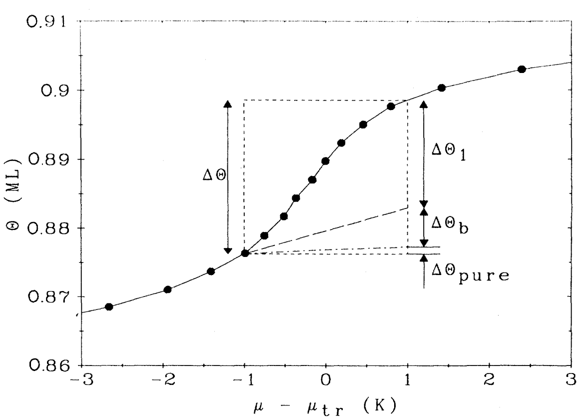

FIG. 9. Expanded plot of an isotherm at $T=125.1$ K in a $\Delta\mu=\pm 3$ K region around the freezing transition. The solid symbols are data points and the solid line is a point-to-point straight interpolation. The box indicates the $\Delta\mu=\pm 1$ K region used in our analysis of the first-order transition. The dot-dashed line is the coverage change due to the pure phase compressibility while the long-dashed line also includes the effect of the temperature independent anomaly. The remaining coverage difference, $\Delta\Theta_1$, is attributed to the first-order transition. See the text for details.

tained by using the data of Fig. 4 and Eq. (3):

$$\Delta\Theta_{\text{pure}} = \Theta_t^2 (K_{\text{sol}} + K_{\text{liq}}) \Delta\mu ,$$

where Θ_t is the coverage at the peak compressibility, K_{sol} (K_{liq}) is the compressibility of the solid (liquid) phase, and $\Delta\mu = 1$ K. This contribution is small in all cases and is shown as the dot-dashed line in Fig. 9. Next, we subtract $\Delta\Theta_b$, the contribution due to the temperature-independent weak anomaly. This is deduced by first parametrizing data in the region $1 < |\Delta\mu| < 40$ K (which excludes the sharp peak) by a Lorentzian form,[18] and using the average of the fitting parameters from all data to integrate the Lorentzian over the $\Delta\mu = \pm 1$ K region

$$\Delta\Theta_b = 2\Theta_t^2 K_L^0 \Gamma_L \arctan(\Delta\mu / \Gamma_L) ,$$

where $K_L^0 = (4.0 \pm 0.2) \times 10^{-3}\ \text{K}^{-1}$ is the peak Lorentzian amplitude and $\Gamma_L = (3.3 \pm 0.1)$ K is the half width at half maximum. Note that the Lorentzian is essentially equal to its peak value over the pertinent interval, so the dashed line showing this contribution in Fig. 9 is straight. The Lorentzian parametrization used here is simply a convenient form which is consistent with the data.[18]

The result of the above analysis is shown in Fig. 10 which shows a roughly linear decrease in $\Delta\Theta_1$ with increasing temperature, and indicates that $\Delta\Theta_1$ goes to zero near $T = 147$ K. Doubling $\Delta\mu$ to ± 2 K yields a result which is consistent within errors with Fig. 10. The slightly negative values of $\Delta\Theta_1$ at $T > 147$ K may indicate a weakening of the nonsingular signature of the continuous transition. Since above $T \sim 147$ K the first-order transition signal is absent, we conclude that the transition has become continuous. At the very minimum, any coexistence region must be extremely narrow.

It should also be emphasized that in the low-temperature region, the Lorentzian fits described above yield a peak which is centered on the first-order peak. The average of the deviations from the position of the compressibility maxima is $\delta\mu = (-0.12 \pm 0.18)$ K which is comparable with our experimental repeatability. We discuss further implications of the data in Sec. V.

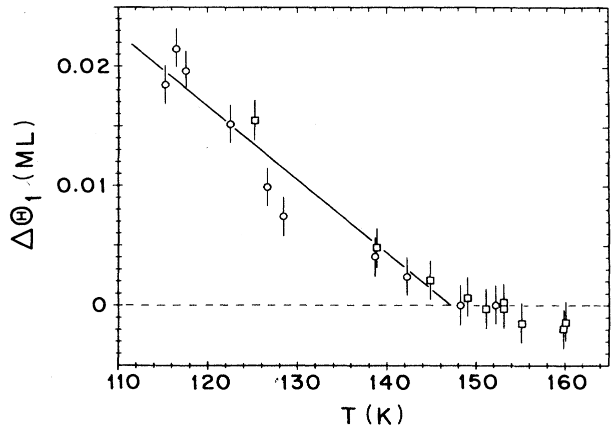

FIG. 10. The width of the first-order coexistence region deduced as discussed in the text. Errors are estimates of our interpolation uncertainty in determining the coverage. The solid line is a guide to the eye. Note that the liquid-solid density difference is less than 2% of a monolayer over the entire region studied.

IV. COMPARISON WITH SCATTERING EXPERIMENTS

In this section, we compare our results with those obtained in high-resolution x-ray scattering experiments on the xenon on graphite system. Our estimate of the multicritical temperature is substantially above the estimate of $T \sim 125$ K obtained in x-ray experiments.[14] It should be emphasized, of course, that in the intervening temperature range, the first-order transition is extremely weak: Fig. 10 indicates that $\Delta\Theta_1 < 1\%$ of a monolayer in this region. We argue below that the scattering data can be interpreted as being consistent with our multicritical temperature. We also attempt here to correlate the thermodynamic and structural trends in the freezing transition signals.

A. Evidence for first-order transitions

The most compelling x-ray evidence for first-order freezing at low temperatures is the observation at $T = 112$ (Ref. 12) and 116 K (Ref. 14) of scattering peaks which are best fit by coexistence lineshapes (that is, a sum of liquid and solid contributions whose width and shape parameters are, at least ideally, determined from scans at neighboring phase diagram points). Both these measurements use ZYX graphite substrates for which signal levels are quite high at synchrotron radiation laboratories and subtle line shape effects can be resolved. The weakness of the first-order character of the transition is evident from two phenomena: (i) coexistence is estimated by Heiney *et al.*[12] to take place over a coverage range of only 2% of a monolayer (note that a 2% coexistence region at $T = 112$ K agrees remarkably well with Fig. 10), and (ii) the width in momentum transfer of the liquid phase contribution to the scattering is small, i.e., the liquid is highly correlated even at these low temperatures. Assuming the fluid is orientationally ordered yields correlation lengths of 54 Å (in a lower resolution experiment),[32] or 30 Å (Ref. 12) at 112 K and of 116 Å at 116 K.[14] Due to the large liquid correlation lengths, the distinction between single-phase fits and coexistence fits is subtle (see Figs. 11 and 12 of Ref. 12) and presumably become more so as the temperature increases.

In x-ray data above $T = 116$ K, no evidence of coexistence has been observed. Attempts have been made, again using ZYX substrates, at 125 (Ref. 14) and 150 K (Ref. 12) to discern a coexistence line shape; the results are inconclusive as might be expected from the fact that no significant deviations are observed in fits to single-phase structure factors. Clearly, the strength of any first-order transition has been reduced compared to that seen at 116 K and the conclusion has been drawn that the transition is "at most, extremely weakly first order."[13,14] This statement is consistent with our observation of the narrowing of the coexistence region.

Short of direct observation of coexistence, can evidence for a change from first order to continuous freezing be

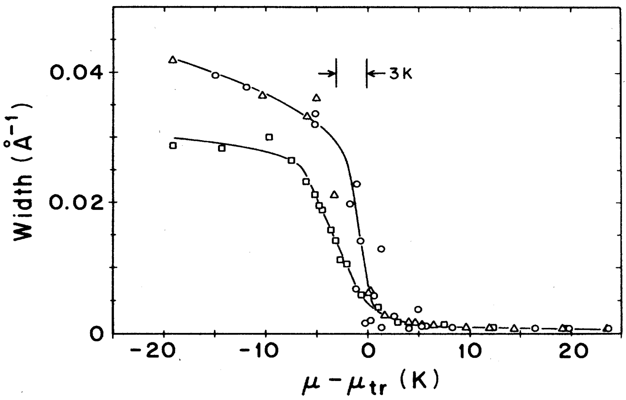

FIG. 11. X-ray scattering linewidths as a function of chemical potential, from three isothermal scans. Symbols are as follows: circles, $T = 125$ K;[14] triangles, $T = 134$ K[14]; and squares, $T = 150$ K.[12] Solid lines are guides to the eye. All widths are determined from fits to the square-root Lorentzian line shape.

observed in the scattering line shape trends? In Fig. 11 we plot fitted x-ray linewidths from three sets of isothermal data, at $T = 125$,[14] 134,[14] and 150 K.[12] All fits are to the square-root Lorentzian functional form which gives a reasonably good fit in all phases. We have computed the chemical potential from the vapor pressures given in the theses of Heiney[12] and Dimon[14] and have attempted to align the points in each data set at which the linewidth starts to increase from the value in the ordered phase. The chemical potential scale is quite expanded so that the behavior near the transition can be observed. As can be seen, the lower temperature sets overlap within the noise, whereas the data at $T = 150$ K appear to have a broader, more gradual transition region. In fact, the low-temperature data have a rapid evolution in linewidth over a region of 2–3 K in $\Delta\mu$, which is the width of the sharp compressibility peaks which we observe. The high-temperature data are at least suggestive of a more continuous evolution in the linewidth. This observation is consistent with our assignment of a multicritical temperature of $T \sim 147$ K.

B. Single crystal experiments

Essentially all the scattering data on single-crystal substrates have been taken along "closed cell" paths.[13,33] It is somewhat difficult to compare such data sets in a way analogous to Fig. 11. As pointed out in the Appendix, the thermodynamic path followed depends on the compressibility of the film, and thus on the extent of heterogeneous smearing. A narrow transition temperature range can be expected wherever the peak compressibility is large as long as the "feedback" term described in the Appendix is small. This should certainly be the case for single-crystal–single-surface substrates. Indeed, Specht *et al.*[13] do not see a coexistence line shape in spite of having taken careful measurements at closely spaced temperatures near the transition at $T = 133.6$ K. If, as one would hope, their sample is more highly homogeneous than exfoliated samples, then we would expect the coexistence temperature interval to be extremely small and very possibly unobservable (again, see the Appendix).

We conclude that the scattering data and our thermodynamic data are not inconsistent. Clearly, a weak first-order transition occurs at low temperatures and the transition becomes even weaker as the temperature is raised. In the region where there is an apparent disagreement over the order of the transition, the thermodynamic data indicate that the transition is extremely weakly first order. We see a coexistence region of width less than 1% of a monolayer. In the same region, single-crystal scattering experiments observe a fluid correlation length of 2000 Å.[13] The fact that no coexistence line shape is observed in scattering experiments may well be an indication that the substrate used is highly homogeneous.

V. DISCUSSION

Through our carefully equilibrated measurements of the two-dimensional compressibility of monolayer xenon on graphite, we have been able to isolate, at low temperatures, a distinct signal of a first-order freezing transition, and we have been able to observe a systematic trend towards a continuous transition as we move to higher temperatures. Combining our measurements with x-ray scattering data indicating the existence of a power-law solid phase up to at least $T = 150$ K, we conclude that the continuous transition can be studied, with minimal interference from second-layer effects, in the interval $147 < T < 155$ K. In the region $120 < T < 147$ K, the width of the liquid-solid coexistence region decreases roughly linearly from 2% of a monolayer to zero. The fact that we are able to detect the signals associated with first-order transitions is due to the fact that we are measuring a quantity, K_T, which has a delta-function response in the coexistence region.

Four different phenomena mark $T \sim 147$ K as a special point in the phase diagram: (i) $\Delta\Theta_1$ becomes zero within our measurement precision, (ii) the shape of the transition anomaly in K_T becomes at most, weakly dependent on temperature, (iii) a break occurs in the coverage-temperature phase diagram, and (iv) the liquid-phase and solid-phase compressibilities at the transition become essentially equal. In addition, it appears that x-ray scattering data suggest that there is a change in the nature of the transition between $T = 134$ and 150 K. Items (i) through (iii) can be expected at the multicritical point, whereas (iv) is an unexpected empirical observation—perhaps just a coincidence, but perhaps a significant statement about the nature of the phases involved. The shape of the $\Delta\Theta_1$ versus T curve (Fig. 10) and the shape of the Θ-T phase diagram [Fig. 5(b)] could be related if a scaling theory of the multicritical point existed. For example, if power laws are assumed, then a tangential approach of the continuous transition line in Fig. 5(b) to the coexistence boundary would imply that the coexistence region should be rounded rather than sharp as indicated in Fig. 10.[34] Unfortunately, the data are insufficiently precise to observe such curvature if it is present near the multicritical point; we have drawn a straight line only because it is the simplest form which is consistent with the data. It is also possible that the free energy near the multicritical point does not contain power laws but instead has some weaker singularities. Clearly, it would be most interesting to see a theory of the multicritical point.

To what extent are our analysis and interpretation regarding the order of the freezing transition unique and reliable? First, it might be argued that the bending of the coverage-temperature phase boundary shown in Fig. 5(b) generates the difference between low- and high-temperature peak shapes. That is, the high-temperature transition signals might be smeared due to the fact that the isothermal path intersects the boundary at a smaller angle than at low temperatures. However, the entire evolution in the compressibility peak height takes place at lower temperatures where the slope is constant, and, in addition, the weak anomaly is seen to have a constant shape from low temperature to high. Second, the composite nature of the peaks in K_T below $T=147$ K is, we think, clear, given the (rather fortuitous) temperature independence of the shape of the weak anomaly. Since the amplitude of the weak anomaly does not scale with the amplitude of the peak compressibility, it is difficult to imagine that this component has anything to do with heterogeneity or finite-size effects. We discuss below a possible origin of the weak component.

It is evident from the scattering data on graphite single crystals[13] that finite-size effects must be important on ZYX and, perhaps, on all substrates. The 2000 Å correlation length which is observed near the transition at $T=133.6$ K is equal to the ZYX surface coherence length. Moving nearer to the multicritical point, the fluid correlation length can only increase (at least on an ideal substrate with no finite size or defect pinning). The extent to which finite size affects our data is not clear. Since such effects usually broaden transition signatures, we find it hard to believe that they are the origin of the sharp spikes seen in K_T at low temperatures. It is possible that the shape of the continuous transition signal is limited by finite size, although, since this signal shows no sign of being singular and is constant over a broad temperature range, we are tempted to think that it is correct in the region around the transition, if not *at* at the ideal transition.

We speculate that the weak anomaly seen in Fig. 8 is characteristic of the multicritical point rather than of the KTHNY-type of transition. The component in question is broad compared to heterogeneity smearing, has a Lorentzian-type shape,[18] and does not change appreciably with temperature over the region we have studied. Furthermore, it appears to be centered under the first-order peak at low temperatures and remains as the only transition signal at $T>147$ K. Evidently, the first-order transition is weak enough in the region studied that the precursive behavior characteristic of the continuous transition is observed before being cut off by the first-order transition. As mentioned earlier, the naive expectation for K_T near a KTHNY transition might be an anomaly similar to that predicted to occur in the heat capacity. In this case, the freezing transition, as observed for instance in a diffraction experiment, should occur on the solid side of the thermodynamic anomaly, not at its center. Given the temperature independence of our observed anomaly, on lowering the temperature into the weakly first-order region, we would expect the first-order signature to appear on the solid side tail of the anomaly. But this is inconsistent with our data. We therefore speculate that the weak anomaly is characteristic of the multicritical transition rather than the KTHNY transition. The lack of growth in the weak component as T increases towards the multicritical point suggests that the multicritical compressibility is not divergent.

If the above speculations are correct, they would suggest a phase diagram with cross-over lines of the type drawn schematically in Fig. 12. Here, we have a large region in which the multicritical point dominates behavior and a narrow, possibly unobservable, KTHNY region. The latter feature is consistent with theoretical arguments given by others.[35] Figure 12 shows no hexatic-to-normal liquid transition. While the sixfold symmetry of the graphite substrate rules out a sharp transition, recent measurements[10] indicate that the substrate plays only a weak role. In this case, a relatively sharp transition from hexatic-to-liquid might be expected. We see no evidence of a second compressibility anomaly, but this might well be due to a lack of significant coupling between the disclination unbinding process and the mechanical properties of the film.

A final point that should be kept in mind concerns the nature of the low-temperature phase whose melting is being observed. Scattering experiments on a variety of forms of graphite substrate[13] as well as other substrates such as Ag(111),[10] yield line shapes which are fit at least as well by a Lorentzian squared functional form as by a power-law line shape. This may be due to the pinning or slow relaxation of unpaired dislocations or substrate boundary effects. The low-temperature phase has been termed an hexatic glass.[13] While pinning effects are weak in the sense that the positional correlation length reaches thousands of Angstroms on single-crystal samples, it is

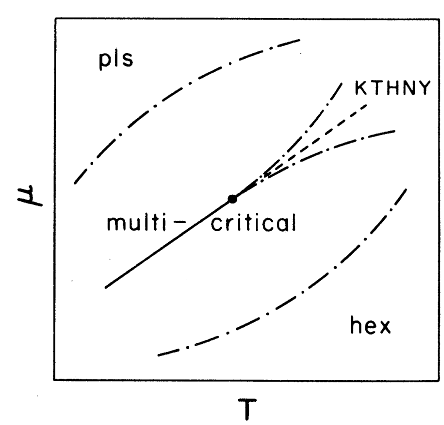

FIG. 12. A speculative phase diagram for xenon on graphite showing cross-over lines (dot-dashed) between noncritical, multicritical, and KTHNY regions. Nomenclature is as in Fig. 5.

possible that the freezing transition is affected in a significant way.

In conclusion , while we feel that there is now strong evidence for the existence of a continuous melting transition in monolayer xenon on graphite, a number of interesting questions remain. To what extent is the compressibility anomaly centered on the point where the positional correlation length diverges? One would like to carry out simultaneous and detailed thermodynamic and scattering experiments near and above the multicritical point. Although evidence exists that the melted phase posesses intrinsic hexatic order,[10,33] one would like to test this evidence by carrying out experiments on additional weakly corrugated, high-quality substrates, ideally, ones without sixfold symmetry. Is the compressibility signal independent of substrate type? Work to address these questions is in progress in our laboratory and others.

ACKNOWLEDGMENTS

We would like to acknowledge helpful conversations with and the encouragement of P. Dimon, R. B. Griffiths, G. Grinstein, P. M. Horn, and K. Strandburg. We thank M. Bretz for a careful reading of an earlier version of the manuscript. This work has been supported by the National Science Foundation (NSF) through Materials Research Laboratory (MRL) Contract No. DMR-8613386.

APPENDIX: DESORPTION IN CLOSED CELL EXPERIMENTS

We present here a thermodynamic expression for the desorption rate with temperature for "closed cell" experiments. The expression can be evaluated using our data and the ideal gas law. We present approximate paths followed through the freezing transition of Xe on graphite under different experimental conditions and discuss the implications.

Consider a closed system which, for simplicity, is at a uniform temperature T. An area A is available for adsorption and the volume is V. The equality of the vapor and film chemical potentials determines the equilibrium configuration of the number of atoms in the film, N_f and the vapor, N_v. Since A and V are fixed, it is convenient to express the chemical potentials as functions of T, and either A and N_f or V and N_v. On changing the temperature by δT, $\delta\mu_f=\delta\mu_v$:

$$\left[\left(\frac{\partial\mu_f}{\partial N_f}\right)_{T,A}+\left(\frac{\partial\mu_v}{\partial N_v}\right)_{T,V}\right]\delta N_f = \left[\left(\frac{\partial\mu_v}{\partial T}\right)_{V,N_v}-\left(\frac{\partial\mu_f}{\partial T}\right)_{A,N_f}\right]\delta T\ , \quad (5)$$

where we have used $\delta N_v=-\delta N_f$. Equation (5) reduces to

$$\frac{\delta\rho_f}{\delta T}=\left[\left(\frac{\partial\mu_v}{\partial T}\right)_{V,N_v}-\left(\frac{\partial\mu_f}{\partial T}\right)_{A,N_f}\right]\Bigg/\left[\frac{1}{\rho_f^2K_T}+\frac{A}{V\rho_v^2K_T^v}\right]\ , \quad (6)$$

where ρ_f is the film density, K_T is the film compressibility and ρ_v and K_T^v are the corresponding vapor quantities. In the ideal gas limit, $\rho_v^2K_T^v=P/(k_BT)^2$. Finally, in convenient laboratory units, we obtain

$$\frac{\delta\Theta}{\delta T}=\frac{\left(\frac{\partial\mu_v}{\partial T}\right)_{V,N_v}-\left(\frac{\partial\mu_f}{\partial T}\right)_{A,N_f}}{\frac{1}{\Theta^2K_T}+10^{-19}\rho_{\mathrm{ML}}\frac{T^2A}{PV}}\ . \quad (7)$$

Here, Θ is in units of the monolayer density, ρ_{ML} is expressed in cm^{-2}, K_T has the units $(\mathrm{ML}^{-1}\mathrm{K}^{-1})$, the μ's are in kelvin, the pressure in Torr and A and V are in cm^2 and cm^3, respectively.

The two terms in the denominator of Eq. (7) compete with each other. In the limit $A/V\rightarrow 0$, the desorption rate is proportional to the film compressibility. This limit would be expected to apply to single-crystal experiments (with the possible exception of a single point on the trajectory, at a first-order transition, where K_T may become extremely large). For finite A/V, the second term (referred to below as the "feedback term") in the denominator reduces the desorption rate: desorbed atoms increase the vapor pressure, providing a negative feedback effect.

We first evaluate, for Xe on graphite near the freezing transition, the terms in the numerator of (7). The first term can be evaluated from the ideal gas form for the vapor chemical potential:

$$\frac{\partial\mu_v}{\partial T}=\frac{\mu_v}{T}-\frac{3}{2}\ . \quad (8)$$

Near the transition, this term ranges from -27 at $T=116$ K to -21 near $T=150$ K. Next, we estimate the film isosteric chemical potential derivative by plotting pairs of isotherms, at neighboring temperatures, against the chemical potential; we then read off chemical potential differences at constant coverage and divide by the temperature difference. Due to the fact that we have not taken data at sufficiently close temperatures, the results are noisy and sparse. However, we can make the following observations. For temperatures away from the freezing transition (at the appropriate coverage), $d\mu_f/dT$ is roughly -5, whereas near the transition there is a weak peak with maximum values of $+3$ (no doubt larger values would be found from more closely spaced isotherms). Note that by a Maxwell relation

$$\left(\frac{\partial\mu_f}{\partial T}\right)_{A,N_f}=-\left(\frac{\partial S}{\partial N_f}\right)_{A,T}\ , \quad (9)$$

where $S(T,A,N_f)$ is the total film entropy. In a uniform phase, the entropy derivative tends to be positive since adding particles makes S larger. But, near a phase transition, adding particles drives the system into the more ordered phase and tends to make the derivative negative. Thus, the peaks in $d\mu_f/dT$ near the freezing transition make sense. However, compared to the range of the corresponding vapor derivative, this term appears small, so below we neglect the film isosteric derivative in (7).

Next, we evaluate the denominator of Eq. (7) and illustrate the variations in the coverage-temperature paths followed under various closed cell conditions. Results are shown in Fig. 13. First, we discuss the single-crystal case where $A/V \rightarrow 0$ and the desorption rate is proportional to K_T. For purposes of illustration, we have taken in Fig. 13 the case of a crystal with heterogeneity smearing comparable to ZYX graphite. In this case, the temperature intervals over which one scans through the coexistence region are 0.02, 0.05, and 0.33 K at $T=120$, 135, and 150 K. Thus, in searching for coexistence phenomena, one must use an extremely fine grid of temperature points. On the other hand, if the single-crystal sample is more homogeneous than ZYX, as one might hope, then the coexistence-temperature interval shrinks as the peak in K_T grows. On an ideal substrate, coexistence occurs only at a single point in temperature. As discussed in the text, this observation, which is really a standard statement of elementary thermodynamics, is necessary to make our interpretation of the compressibility data consistent with the scattering measurements on single crystals.[13]

Next, we consider a large area per volume case: ZYX exfoliated graphite in a small volume cell. A one gram piece of ZYX has $A \sim 3\times10^4$ cm^2; a minimum vapor volume would be of the order of 10 cm^3 (this is roughly the size of the sample cell used in Ref. 12; on the other hand, the actual volume accessible to the vapor is larger since tubing connecting the sample cell to the room-temperature gas-handling system should be included). For monolayer Xe, $\rho_{ML} \sim 5.5\times10^{14}$ cm^{-2}. Thus, $10^{-19}\rho_{ML}A/V \sim 0.2$ Torr/K. At $T=120$ K, where the transition vapor pressure is ~ 0.01 Torr, the variation in K_T has essentially no effect on the path in spite of the large peak in the coexistence region. The coexistence region is traversed in a broad, ($\Delta T \sim 5-7$) K temperature interval. At $T=135$ K, a slight increase in slope is visible in the coexistence region, but the reduction in the feedback term due to increased vapor pressure is the major factor in narrowing the transition interval to $\Delta T < 1$ K. At $T=150$ K, where the transition vapor pressure is 35 Torr, desorption is ineffective in increasing P and a significant anomaly is present in the path near the transition. The transition signature should be essentially the same for ZYX as for a single crystal. Larger vapor volumes will reduce the temperature interval over which the transition takes place. The intervals indicated in Fig. 13 are somewhat larger than what has been observed experimentally,[12] presumably due to our underestimation of the vapor volume.

In single-crystal experiments,[10,13] the feedback term is negligible, and results do not depend on sample cell geometries. Still, it should be kept in mind that, since the phase boundary occurs at almost constant coverage, the driving force for passing through the freezing transition is desorption. Clearly, if one wants to fit theoretical functional forms to observed parameter trends, it is best to follow the simple isothermal path rather than the closed cell paths described here.

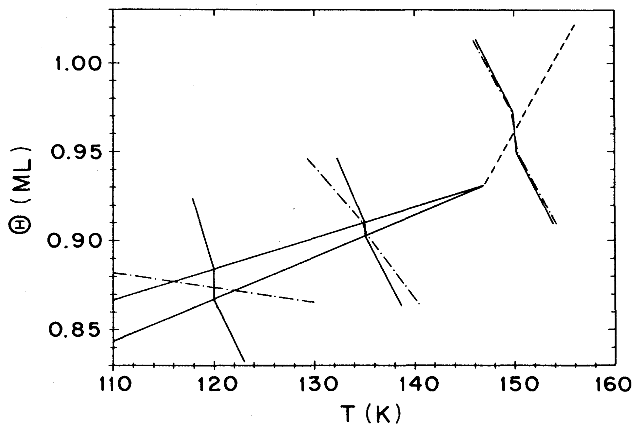

FIG. 13. A schematic illustration of paths followed in closed cell-temperature scan experiments. As detailed in the text, the dot-dashed lines are for a large A/V system, the solid lines are for $A/V \rightarrow 0$. The piecewise linear paths are used for simplicity. The extent in coverage of the solid lines corresponds to the coverage interval spanned by our isothermal paths over $\Delta\mu = \pm 50$ K of the transition. The phase boundaries are schematic, but represent the simplest interpretation of our data.

*Permanent address: Lawrence Livermore Laboratory, Box 808 L-278, Livermore, CA 94550.

[1]J. M. Kosterlitz and D. J. Thouless, J. Phys. C **6**, 1181 (1973); J. M. Kosterlitz, *ibid.* **7**, 1046 (1974).

[2]B. I. Halperin and D. R. Nelson, Phys. Rev. Lett. **41**, 121 (1978); **41**, 519(E) (1978); D. R. Nelson and B. I. Halperin, Phys. Rev. B **19**, 2457 (1979).

[3]A. P. Young, Phys. Rev. **19**, 1855 (1979).

[4]L. D. Landau, *Collected Papers of L. D. Landau* (Pergamon, New York, 1965).

[5]See for example, N. Boccara, *Symetries Brisees* (Herman, Paris, 1976).

[6]N. D. Mermin and H. Wagner, Phys. Rev. Lett. **17**, 1133 (1966); N. D. Mermin, J. Math. Phys. **8**, 1061 (1967); Phys. Rev. **176**, 250 (1968).

[7]K. J. Strandburg, Rev. Mod. Phys. **60**, 161 (1988).

[8]As noted in the discussion section, pinning, impurities and/or slow equilibration of topological defects appear to limit the divergence of the positional correlation length. It has been proposed that the low-temperature phase is actually an hexatic glass. However, the distinction is a subtle one since the correlation length reaches ~2000 Å before saturation in experiments on single-crystal graphite substrates (see Ref. 13).

[9]C. A. Murray and D. H. Van Winkle, Phys. Rev. Lett. **58**, 1200

(1987).

[10]N. Greiser, G. A. Held, R. Frahm, R. L. Greene, P. M. Horn, and R. M. Suter, Phys. Rev. Lett. **59**, 1706 (1987).

[11]At low temperatures, the substrate does play an important role; see for example, H. Hong, R. J. Birgeneau, and M. Sutton, Phys. Rev. B **33**, 3344 (1986); H. Hong, A. Mak, C. Peters, R. J. Birgeneau, and P. M. Horn, in National Synchrotron Light Source Annual Report 1986, Report No. BNL 52045, p. 409; P. S. Schabes-Retchkiman and J. A. Venables, Surf. Sci. **105**, 536 (1981); T. Halpin-Healy and M. Kardar, Phys. Rev. B **34**, 318 (1986).

[12]P. A. Heiney, P. W. Stephens, R. J. Birgeneau, P. M. Horn, and D. E. Moncton, Phys. Rev. B **28**, 6416 (1983); P. A. Heiney, Ph.D. thesis, Massachusetts Institute of Technology, 1983.

[13]E. D. Specht, R. J. Birgeneau, K. L. D'Amico, D. E. Moncton, S. E. Nagler, and P. M. Horn, J. Phys. (Paris), Lett. **46**, L561 (1985).

[14]P. Dimon, P. M. Horn, M. Sutton, R. J. Birgeneau, and D. E. Moncton, Phys. Rev. B **31**, 437 (1984); P. Dimon, Ph.D. thesis, University of Chicago, 1984.

[15]C. Tessier, doctoral thesis, L'Universite de Nancy I, 1983.

[16]M. R. Bjurstrom, J. Albert Jin, Y. P. Feng, and M. H. W. Chan, Bul. Am. Phys. Soc. **32**, 398 (1987).

[17]J. A. Litzinger and G. A. Stewart, *Ordering in Two Dimensions,* edited by S. K. Sinha (North-Holland, Amsterdam, 1980).

[18](a) N. J. Colella and R. M. Suter, Phys. Rev. B **34**, 2052 (1986); (b) N. J. Colella, Ph.D. thesis, Carnegie-Mellon University, 1986.

[19]R. M. Suter, N. J. Colella, R. Gangwar, and W. Wang, Rev. Sci. Instrum. **58**, 462 (1987).

[20]The details of our method for letting gas into the gas-handling system were omitted from Ref. 19. We use a model SS-4BG-TW Nupro valve with a "U" series air operated opener. By backing the valve stem out of the opener, we push the air diaphragm essentially to its fully open position with the value still closed. When air is then introduced into the opener, the value is cracked open only slightly, allowing a slow leaking of gas into the system and, thus, a repeatable and adjustable inlet charging. This rather *ab hoc* arrangement works remarkably well.

[21]R. J. Birgeneau, P. A. Heiney, and J. P. Pelz, Physica **109-110B**, 1785 (1982).

[22]T. Takaishi and Y. Sensui, Trans. Faraday Soc. **59**, 2503 (1963).

[23]J. G. Dash and R. D. Puff, Phys. Rev. B **24**, 295 (1981).

[24]R. E. Ecke, J. G. Dash, and R. D. Puff, Phys. Rev. B **26**, 1288 (1982).

[25]J. J. Hamilton, Phys. Rev. B **32**, 4760 (1985).

[26]R. M. Suter, N. J. Colella, and R. Gangwar, Phys. Rev. B **31**, 627 (1985).

[27]See Ref. 37 in D. R. Nelson and B. I. Halperin, Phys. Rev. B **19**, 2457 (1979).

[28]A. Thomy and X. Duval, J. Chem. Phys. **66**, 1966 (1969); **67**, 286 (1970); **67**, 1101 (1970).

[29]In Ref. 18 we used a slightly different monolayer definition. The difference between our previous definition and the conventional one is essentially the same as the degree of variation with temperature of the takeoff in K_T shown in Fig. 2. Hence, we now adopt the conventional definition.

[30]R. B. Griffiths, Phys. Rev. Lett. **24**, 715 (1970).

[31]R. E. Ecke, J. Ma, A. D. Migone, and T. S. Sullivan, Phys. Rev. B **33**, 1746 (1986).

[32]E. M.Hammonds, P. Heiney, P. W. Stephens, R. J. Birgeneau, and P. M. Horn, J. Phys. C **13**, L301 (1980).

[33]S. E. Nagler, P. M. Horn, T. F. Rosenbaum, R. J. Birgeneau, M. Sutton, S. G. J. Mochrie, D. E. Moncton, and R. Clarke, Phys. Rev. B **32**, 7373 (1985).

[34]R. B. Griffiths (private communication).

[35]J. L. Cardy, Phys. Rev. B **26**, 6311 (1982).